ELSEVIER

Materials Science and Engineering A 479 (2008) 58–64

MATERIALS SCIENCE & ENGINEERING A

www.elsevier.com/locate/msea

Effect of wall microstructure and morphometric parameters on the crush behaviour of Al alloy foams

Francesca Campana [a], Daniela Pilone [b,*]

[a] *Dipartimento di Meccanica e Aeronautica, Sapienza Università di Roma, Via Eudossiana 18, 00184 Roma, Italy*
[b] *Dipartimento ICMMPM, Sapienza Università di Roma, Via Eudossiana 18, 00184 Roma, Italy*

Received 21 March 2007; received in revised form 8 June 2007; accepted 12 June 2007

Abstract

Three different aluminium foams, manufactured by compact powder technology starting from 7075, 6061 and AlSi7 alloys were studied by performing microstructural and morphometric analyses, with the aim of explaining their different behaviour during axial crushing. Void distribution coupled with material microstructure justifies the behaviour of load–displacement curves obtained during axial crushing of the foams. The results show that 7075 alloy seems to be the material having the best behaviour during crushing, at least when the foam is removed of the external walls. Despite that outer skin presence coupled with the intrinsic brittle behaviour of this alloy may cause instability, if it is used to fill hollow components like crashboxes. During deformation process 6061 and AlSi7 alloys that are more ductile, give in and maintain contact adapting to the encasement deformation.

Keywords: Aluminium foam; Aluminium alloy; Crashworthy design; Heat treatment; Microstructure

1. Introduction

Over the past 10 years there has been interest in the production and characterisation of lightweight metallic foams [1–5]. These materials have great potential for a number of applications in the automotive, railway and aerospace industry. In particular, they are interesting in the crashworthy design to produce components able to withstand loads, dissipate kinetic energy and minimise forces and accelerations experienced by components during the application of dynamic loads.

Several methods have been used to produce metallic foams: the most common one is based on powder metallurgy. After hot pressing the metallic powder and the foaming agent (usually TiH_2), the precursor is foamed by heating it up above the melting temperature. This process appears interesting since it allows the production of complex shapes by varying the die geometry. It also allows in situ foaming by filling hollow elements with the powder and by heating them up at the desired temperature. Although the latter process could be very interesting from the technological point of view as it reduces the costs related to foam insertion in complex shapes, structural problems can arise from residual stresses due to the different thermal expansion between foam and hollow element.

Another disadvantage related to the use of metallic foams is their inhomogeneity, pore shape and distribution anisotropy as well as metallurgical state and defects. Size, shape and distribution of cells are strictly connected to the process parameters used during the foaming process. A number of papers is available in literature concerning the process parameters optimisation for aluminium foam manufacturing and the study of aluminium foam formation: these works are focused on how the foam emerges from the liquid, how it changes with time and what mechanisms are responsible for its formation [6–8].

In order to use foamed metals as a tailored material, it is of paramount importance to know the relationship between morphological and mechanical properties. So far, studies on foam mechanical properties have been carried out on specimens characterised by a porosity fraction varying over the range 70–90%, which have great usable strain as energy absorber [9]. Generally speaking, it can always be found a strong correlation between absorbed energy and foam density, while the selected alloy affects both the values of absorbed energy and the load uniformity during crushing [10]. This behaviour is affected by bulk material microstructure and type of load (static or dynamic).

* Corresponding author. Tel.: +39 0644585879; fax: +39 0644585641.
E-mail address: daniela.pilone@uniroma1.it (D. Pilone).

0921-5093/$ – see front matter © 2007 Elsevier B.V. All rights reserved.
doi:10.1016/j.msea.2007.06.040

There are many papers available that studied the strain dependence of mechanical properties of foams [11–14]. It has been reported that the specific energy absorption of Alcan aluminium foam is independent of applied strain rate in the range 10^{-3} to $10^{3}\ s^{-1}$ [14] and that the plateau stress obtained for Alulight and Duocell foams is almost insensitive to strain rate, for strain rates up to $5000\ s^{-1}$ [12].

Determining a correlation between foam morphology and mechanical behaviour requires the knowledge of 2D and 3D-foam architecture. Resolving the structure includes several methods, studied over the past few years, such as embedding the foam in a coloured resin for contrast or using micro-computed tomography, although the latter method is not yet standardised [15]. Despite the extensive work carried out on this topic there is uncertainty about the role of foam morphology and skin thickness in affecting mechanical properties.

A further important factor affecting the mechanical response of metallic foams, when a static or a dynamic load is applied, is the cell wall and skin microstructure, i.e. size and distribution of secondary phases can dramatically influence the material performance. Few papers concerning the effect of cell wall microstructure on the deformation of aluminium based foams are available in literature [16–18]: it is concluded that cell wall ductility and toughness are impaired by a high volume fraction of coarse eutectic or brittle particles and that a careful selection of heat treatment parameters allows to customise the foam properties.

The aim of the present work is to analyse the combined effect of morphometric parameters and wall microstructure on foam mechanical properties relevant to crushing energy absorption.

2. Experimental procedure

Aluminium based foams, investigated in this work, are produced and supplied by IFAM in Bremen, Germany. They are manufactured by compact powder technology. All the specimens have square base section (45 mm × 45 mm) and 100 mm height (Fig. 1). Their size and shape were established according to common practice in bumper crashbox design.

The selected alloys used in this work were Al 6061, Al 7075 and AlSi7. Their nominal composition is reported in Table 1.

The research was carried out by using the following methodologies: image analysis of cell distribution inside the specimen, microstructural examination by SEM/EDS (energy dispersive spectroscopy) and mechanical characterisation by crushing.

All foam specimens were characterised in terms of density using a calliper and an Orma microbalance.

Several samples, for every considered alloy, were sectioned minimising cell wall damage. The surfaces were painted using a black dye in order to obtain a good contrast, essential for image analysis. The specimens were ground with a series of SiC papers and afterwards polished with 1 and 0.3 μm alumina. Image analysis was carried out using Leica QWin software: cell size, roundness and mean area were determined at different distances from the ingot surfaces.

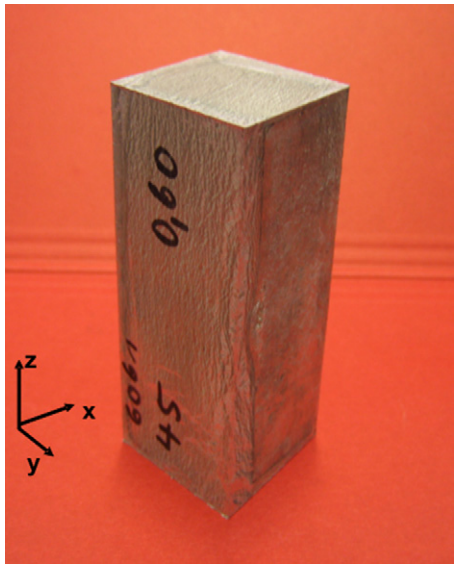

Fig. 1. Macrograph of a foam specimen.

Microstructural examination of polished cross-sections was performed using a scanning electron microscope and compositional analyses were performed using EDS.

Uni-axial compression tests were carried out on a MTS testing machine (max load 25 tonnes). Tests were conducted under displacement control with a cross-head speed of 0.5 mm/s (quasi-static load condition). Considering that mechanical properties of foams are almost insensitive to strain rate for strain rates up to $1000\ s^{-1}$, quasi-static tests allow to assess foam behaviour in case of low speed manoeuvring collisions (less than 15 km/h). Further tests were carried out with a speed 100 times greater just to confirm that in this speed range no relevant strain rate effect occurs. The main output of this kind of test is a load–displacement curve. This curve allows extrapolation of important indicators, such as initial peak load, mean force, specific energy absorption and material efficiency, which is calculated as the ratio between mean force and peak load. Because of the inhomogeneous cell distribution that causes scattered results, mechanical tests were carried out on more than three specimens for each foam and the obtained data were averaged out.

Table 1
Nominal composition (wt.%) of the tested alloys

	Mg	Si	Cu	Cr	Mn	Zn	Fe
6061	0.8–1.2	0.4–0.8	0.15–0.4	0.04–0.35	0–0.15	–	–
7075	2.1–2.9	0–0.40	1.2–2.0	0.18–0.28	0–0.30	5.1–6.1	–
AlSi7	0.25–0.40	6.5–7.5	0–0.10	–	0–0.4	0–0.10	0–0.7

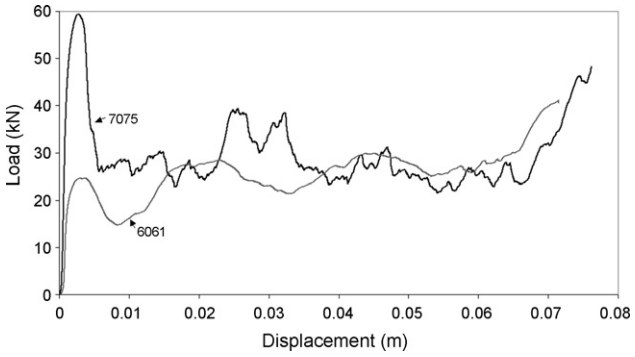

Fig. 2. Crushing behaviour of 7075 and 6061 foam specimens (nominal density 900 kg/m^3).

3. Results and discussion

In the first part of this research project foam mechanical characterisation of 7075 specimens, revealed some deviations from the foam's ideal absorption behaviour (Fig. 2). Their load–displacement curves show large oscillation coupled with jagged behaviour, characteristic of low efficiency and high dispersion absorption capability. These effects are respectively connected to the outer specimen's wall thickness and the alloy's intrinsic brittle behaviour. During the crush test part of the energy is spent to compress the walls, which behave as an outer brittle tube filled by foam. All the specimens have outer walls due to the foaming process. Different 7075 and 6061 alloy specimens were cut both in cross and longitudinal sections for a qualitative assessment of the outer wall thickness. Its width is randomly distributed and varies from few tenths of millimetres to 2 mm (Fig. 3). In samples characterised by almost uniform and large skin thickness in the load direction, peaks occur before the outer walls could be crushed. Fig. 2 clearly shows this phenomenon. The large oscillations around the mean load are the result of the external wall crushing. The curves obtained for 6061 alloy specimens are smoother because 6061 alloy is less brittle. This observation suggested that a thorough investigation on outer wall's microstructure and thickness distribution could be crucial in understanding and interpreting the mechanical behaviour of the studied samples.

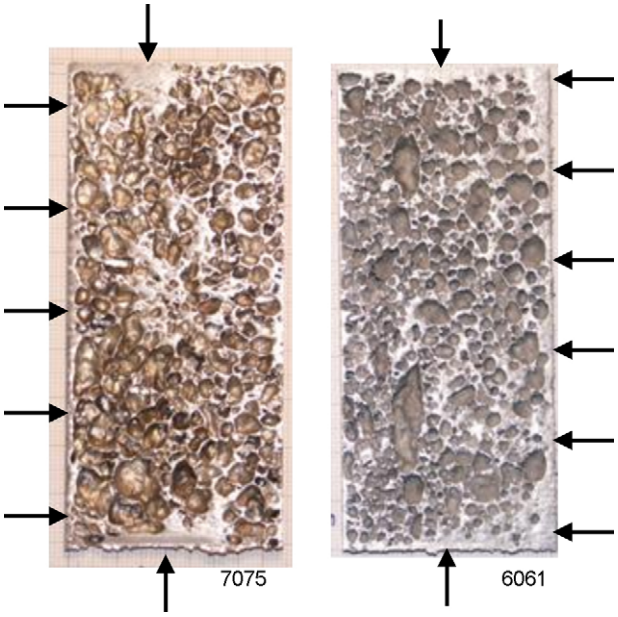

Fig. 3. Macrographs showing outer wall thickness distribution in 6061 and 7075 alloy foams.

3.1. Morphological examination

The morphological examination was performed on several specimens for every considered alloy. Due to the irregular cell's shape and distribution, evident to a naked eye examination, it was decided to divide the outer walls, cut along the z-direction, into three different pieces. Average void density and cell roundness were determined for every considered area in order to evaluate a possible correlation between cell shape irregularity and its position along the specimen.

Void density, D_v, was given by:

$$D_v(\%) = \frac{\Sigma A_i}{A_{tot}} \times 100 \quad (1)$$

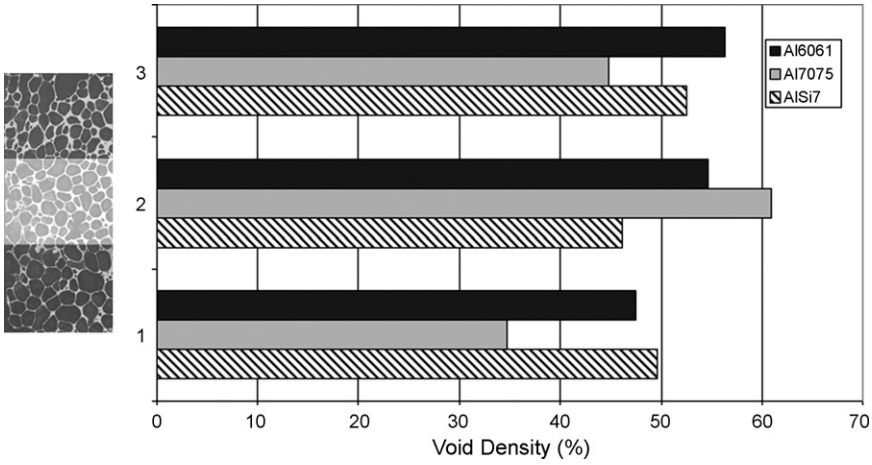

Fig. 4. Void density distribution along the z-direction calculated for 7075, 6061 and AlSi7 alloys.

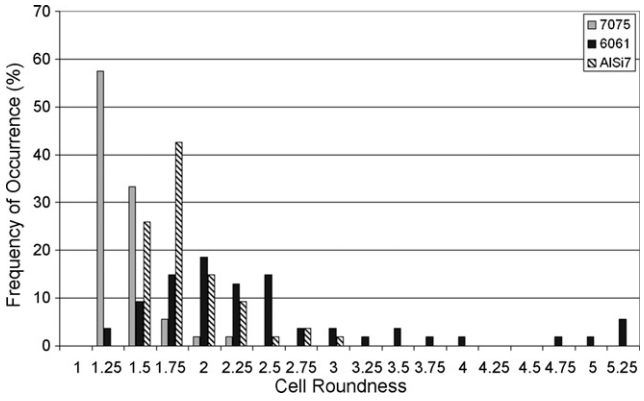

Fig. 5. Cell roundness distribution in 7075, 6061 and AlSi7 alloy specimens.

where A_i stands for ith void area and A_{tot} for the investigated total area.

Cell roundness, R, measures the morphological aspect of cavities. It is an adimensional value defined by:

$$R = \frac{L}{4\pi A_i \times 1.064} \quad (2)$$

where L is the cell perimeter and 1.064 is a factor that takes into account the error introduced in the area calculation by the digitalisation of the image, during which continuous perimeters are approximated by discrete rectangles. R is equal to 1 when the shape is circular, while voids that differ from circles are characterised by R-values greater than 1.

Void density values, calculated for specimens all having a nominal density equal to 750 kg/m^3, are reported in Fig. 4. The results are grouped into three sets, one for each area where the computation was done.

AlSi7 is found to have the most uniform void density along the specimen height ($49.4 \pm 3\%$), followed by 6061 ($52.8 \pm 4.73\%$). 7075 alloy has more voids in the specimen's centre part (area 2: 60.9%) with a mean value of $46.8 \pm 13.2\%$.

Fig. 5 shows the frequency of occurrence $f(R)$ of a given cell roundness R, against R, in specimens made of different alloys. In terms of roundness, 7075 and 6061 alloys present the most regular cell's shape, with an average R-value equal to 1.3 and 2.2, respectively. AlSi7 is characterised by a mean R-value equal to 2.

AlSi7 data are distributed, indicating that cell shapes of AlSi7 specimens vary over the range 1.5–3. 7075 specimens have quite round cells: R varies mostly between 1.25 and 1.75. 6061 alloy has the greatest mean roundness value among the three studied alloys: cells are characterised by a roundness factor varying over all the considered range.

The macrographs reported in Fig. 6 clearly show the inhomogeneity of void shape and distribution in AlSi7 specimens. As it can be observed the outer walls cannot be clearly identified. In fact the outer part of AlSi7 specimens is quite compact, although it contains a very large number of small voids. The inner part is characterised by large voids anisotropically distributed.

Image analysis highlighted also that foams made of different alloys are characterised not only by different cell shape and distribution, but also by different cell areas. In fact the mean cell area calculated for 7075, 6061 and AlSi7 foams are 11.03, 4.04 and 3.46 mm^2, respectively. 7075 alloy foam is the one characterised by the biggest and almost circular cells.

3.2. Microstructural characterisation

Cell wall and skin microstructure can dramatically affect the mechanical response of metallic foams, in fact size and distribution of secondary phases can influence the material performance. To improve the contrast between the different phases in the cell walls and in the skins back-scattered mode image was used.

Microscopic investigations highlighted that, independently of the considered alloy, the outer skins contain a higher volume fraction of secondary phases in comparison with the cell's walls. This is probably due to different cooling rates in different areas of such a complex system.

SEM inspection of 6061 alloy foams revealed the presence in the skin microstructure of a phase having Chinese script morphology (Fig. 7). Chinese script α-(Fe,Si) is one of the most common and influential intermetallic phases found in

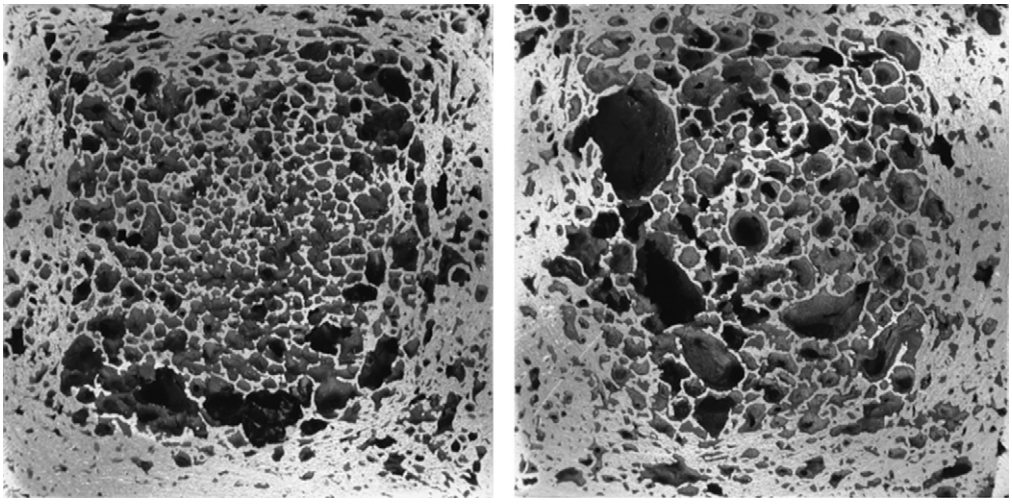

Fig. 6. Macrographs showing void distribution on two cross-sections of AlSi7 foams.

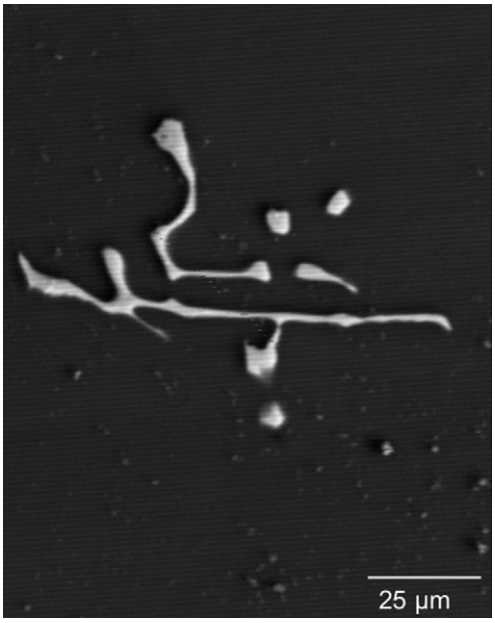

Fig. 7. SEM back-scattered image showing the Chinese script intermetallic phase found in the 6061 foam skin.

aluminium–silicon alloys [19]. EDS analyses identified that phase as $(Fe,Cr)_3SiAl_{12}$. A phase having the same chemical composition, but a polygonal shape, was found in the cell wall microstructure. The low cooling rate in the ingot inner part favours diffusion processes and then the growth of coarse intermetallic phases.

SEM analyses carried out on 7075 alloy highlighted that two intermetallic phases were formed: a Fe rich phase, which was compact and platelet shaped, and a Cu rich phase with a dendritic morphology (Fig. 8).

AlSi7 alloy after foaming shows typical microstructure of cast Al–Si alloy with light α-Al grains and heterogeneous Al–Si regions with their characteristic dark silicon needles (Fig. 9).

Microscopic investigation revealed also the presence of large titanium particles randomly distributed within the cell walls.

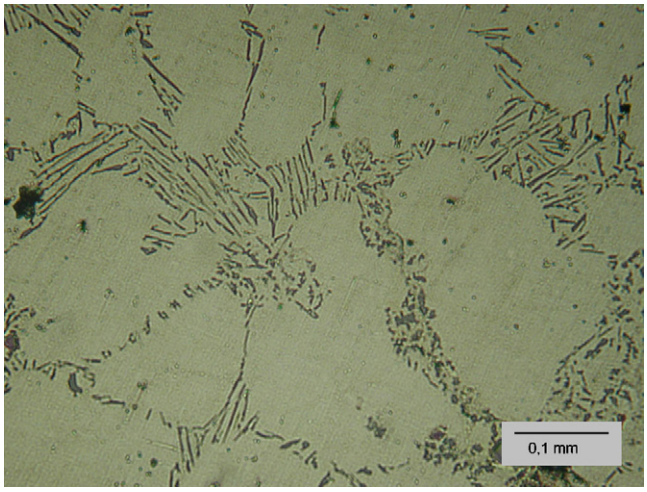

Fig. 9. Micrograph showing AlSi7 foam microstructure.

These particles were surrounded by a sheath of a Si–Ti phase (Fig. 10b and c) produced during the foaming process when TiH_2 reacts to release hydrogen. The presence of these partially reacted particles within the cell walls suggests that the foaming process was not efficient.

Thorough selection of alloy composition and manufacturing process parameters can strongly affect alloy microstructure and cell shape, i.e. silicon needles characterising Al–Si alloys probably influence surface tension and then cell shape.

3.3. Mechanical characterisation

The compressive stress–strain curve of aluminium alloy foams, under quasi-static compression, exhibits three deformation characteristics, similar to those of other metal foams. An initial linear-elastic region followed by a load-softening region to a plateau region where successive bands of cells deform plastically and collapse. Beyond the plateau cells are compacted together.

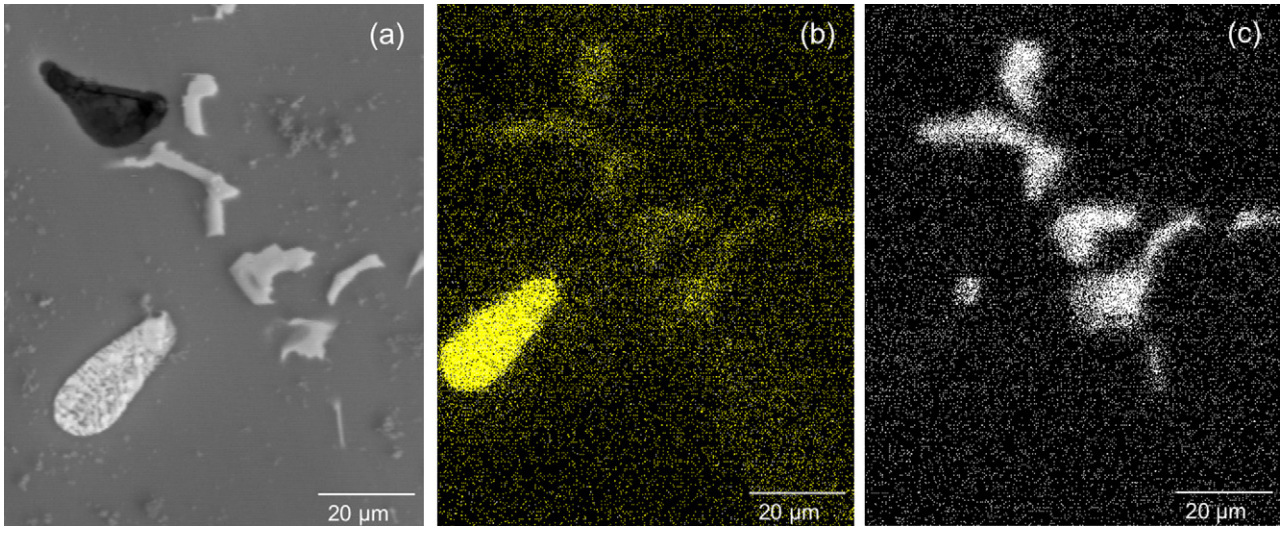

Fig. 8. Back-scattered SEM image (a) showing two different intermetallic phases found in 7075 alloy and X-ray maps highlighting copper (b) and iron (c) distribution.

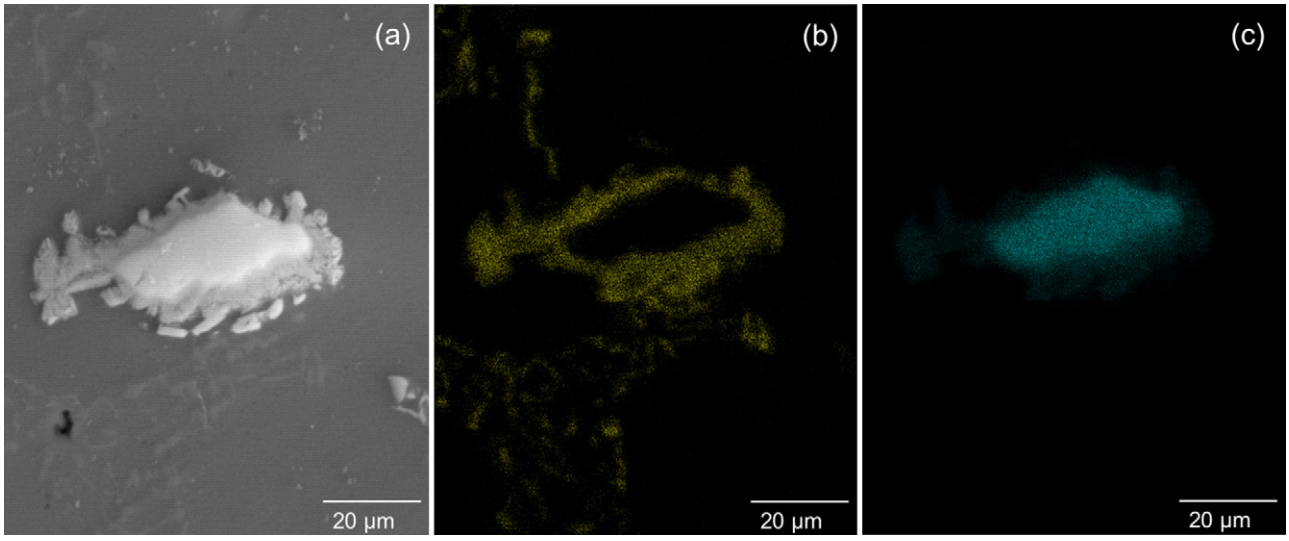

Fig. 10. Back-scattered SEM image of AlSi7 foam (a) showing a blocky Ti particle and X-ray maps highlighting silicon (b) and titanium (c) distribution.

Due to the outer walls microstructure, characterised by fine intermetallic particles, 7075 and 6061 alloys show unstable behaviour that causes a decrease in energy absorption efficiency due to initial peaks and large load variation in the plateau region. AlSi7 is more ductile and voids are located mainly in the centre of specimens, while in the outer part there is a quasi-homogeneous region that during crushing may strain harden. This explains why the AlSi7 load–displacement curves show no initial peak, no oscillations and a pronounced strain-hardening slope. Table 2 summarises the global values achieved for all the alloys.

Some specimens made of 6061 and 7075 alloys were removed of their outer skins to study their mechanical behaviour (Fig. 11). The comparison among compressive load–displacement curves obtained for all the alloys highlights that, after the initial linear-elastic region, for AlSi7 and 6061 alloys the stress increases slowly as plastic deformation proceeds. 7075 behaviour still shows stress oscillations superimposed upon constant stress level. These oscillations are typically associated with brittle behaviour. More ductile alloy foams, such as AlSi7 foams, fail with a smooth rising curve and the failure is mainly due to cell walls bending [18].

The study of a number of frames taken during the test sequence highlighted the foam's behaviour during crush tests. Cell walls of 7075 alloy foam collapse in the areas where the walls are thinner and the failure starts from pre-existing cracks. External skin crumbles during compression tests, so witnessing the brittle behaviour of 7075 outer walls.

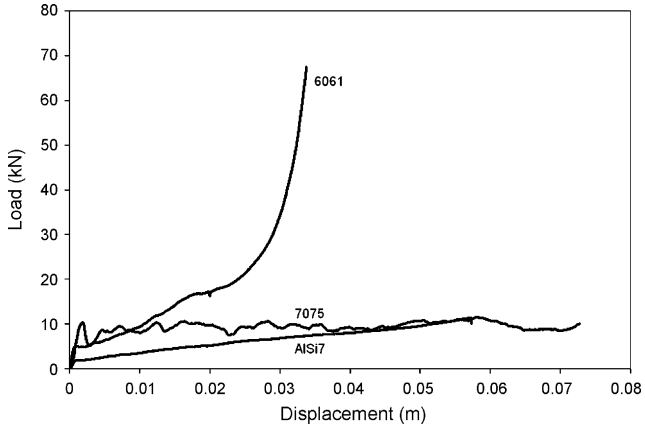

Fig. 11. Load–displacement curves for 6061, 7075 and AlSi7 alloy specimens removed of the external skin.

Energy absorption capacity of metallic foams is key to make them interesting in the crashworthy design. Fig. 12 shows the energy absorption capacities per unit mass of 6061, 7075 and AlSi7 alloy foams. 7075 specimens, despite the brittle behaviour witnessed by the jagged curves, show a linear absorption capacity, while the other two alloys seem to be less efficient in the first compression stages. In the case of AlSi7 this is due to strain hardening.

On the ground of these results 7075 alloy seems to be the material having the best characteristics during crushing, at least when the foam is removed of the external walls. Outer skin presence coupled with its intrinsic brittle behaviour may cause

Table 2
Absorption characteristics of specimens having the same nominal density (700 kg/m^3)

	Peak load (kN)	Mean force (kN)	Efficiency	Specific energy (J/g)
6061	35.05 ± 5.3	29.82 ± 5.5	0.85 ± 0.05	12.7 ± 1.4
7075	66.9 ± 6.7	43.68 ± 4.4	0.65 ± 0.06	17.6 ± 1.8
AlSi7	–	25.42 ± 4.1	–	10.5 ± 1.6

The specific energy is calculated considering 60 mm displacement.

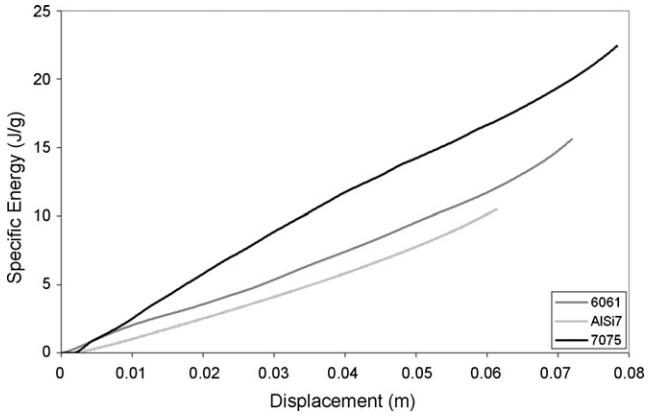

Fig. 12. Energy absorption capacity of 6061, 7075 and AlSi7 alloy specimens removed of the external skin.

instability if that alloy is used to fill hollow components like crashboxes. During deformation process 6061 and AlSi7 alloys that are more ductile, give in and maintain contact adapting to the encasement deformation.

4. Conclusions

Three different aluminium foams, manufactured by compact powder technology starting from 7075, 6061 and AlSi7 alloys, were studied with the aim of explaining their different behaviour during axial crushing. The manufacturing process and the alloy composition induce a scattered voids distribution, both in terms of shape and location. 7075 and 6061 specimens show the most regular void shape (roundness index equal to 1.3 and 1.7, respectively); AlSi7 foam is characterised by cell roundness varying over a wide range. The first two alloys generally present outer walls of compact material with thickness varying from 0.5 to 2 mm. During crushing the walls presence produces load oscillations that decrease the energy absorption efficiency. Microstructural examination of 6061 and 7075 alloy foams highlighted that the outer skins contain a higher volume fraction of secondary phases in comparison with the cell's walls. This characteristic determines the brittleness of the external skin, especially in 7075 alloy foams.

AlSi7 specimens do not have such behaviour because voids are mainly located in the specimen core, surrounded by a quite compact alloy layer thicker than 5 mm. This morphological distribution, coupled with the material microstructure, justifies the smoothness and the pronounced strain-hardening slope of AlSi7 load–displacement curves.

Reducing microstructure and void heterogeneity may increase foam stability during crushing. This reduction can be obtained only by optimising manufacturing process parameters.

References

[1] P.J. Tan, S.R. Reid, J.J. Harrigan, Z. Zou, S. Li, J. Mech. Phys. Solids 53 (2005) 2174–2205.
[2] E. Koza, M. Leonowicz, S. Wojciechowski, F. Simancik, Mater. Lett. 58 (2003) 132–135.
[3] D.P. Papadoupulos, I.Ch. Konstantinis, N. Papanastasiou, S. Skolianos, H. Lefakis, D.N. Tsipas, Mater. Lett. 58 (2004) 2574–2578.
[4] B.V. Krishna, S. Bose, A. Bandyopadhyay, Mater. Sci. Eng. A452/A453 (2007) 178–188.
[5] J. Zhou, W.O. Soboyejo, Mater. Sci. Eng. A369 (2004) 23–35.
[6] I. Duarte, J. Banhart, Acta Mater. 48 (2000) 2349–2362.
[7] W. Ha, S.K. Kim, H.-H. Jo, Y.-J. Kim, Mater. Sci. Technol. 21 (2005) 495–499.
[8] G. Costanza, R. Montanari, M.E. Tata, La Metall. Ital. 6 (2005) 41–47.
[9] S.W. Youn, C.G. Kang, Metall. Mater. Trans. A 35 (2004) 2419–2426.
[10] G.B. Broggiato, F. Campana, F. Mascioni, G. Santucci, in: J. Banhart, M.F. Ashby, N.A. Fleck (Eds.), Proceedings of METFOAM 2001, Bremen (Germany), June, 2001, pp. 359–364.
[11] G.B. Broggiato, F. Campana, L. Peroni, in: J. Banhart, N.A. Fleck, A. Mortensen (Eds.), Proceedings of METFOAM 2003, Berlin (Germany), June, 2003.
[12] V.S. Deshpande, N.A. Fleck, Int. J. Impact Eng. 24 (2000) 277–298.
[13] D. Ruan, G. Lu, F.L. Chen, E. Siores, Compos. Struct. 57 (2002) 331–336.
[14] L.D. Kenny, Mater. Sci. Forum 217–222 (1996) 1883–1890.
[15] O.B. Olurin, M. Arnold, C. Körner, R.F. Singer, Mater. Sci. Eng. A328 (2002) 334–343.
[16] J. Zhou, Z. Gao, A.M. Cuitino, W.O. Soboyejo, Mater. Sci. Eng. A 386 (2004) 118–128.
[17] A.E. Markaki, T.W. Clyne, Acta Mater. 49 (2001) 1677–1686.
[18] D. Lehmhus, J. Banhart, Mater. Sci. Eng. A249 (2003) 98–110.
[19] M.V. Kral, Mater. Lett. 59 (2005) 2271–2276.